Pfeffer, S. R., Stahl, S. J., & Chamberlin, M. J. (1977) *J. Biol. Chem. 252*, 5403–5407.
Reznikoff, W. S. (1976) in *RNA Polymerase* (Losik, R., & Chamberlin, M., Eds.) pp 441–454, Cold Spring Harbor Press, Cold Spring Harbor, NY.
Roeder, R. G. (1976) in *RNA Polymerase* (Losik, R., & Chamberlin, M., Eds.) pp 285–329, Cold Spring Harbor Press, Cold Spring Harbor, NY.
Rosenvold, E. C., & Honigman, A. (1977) *Gene 2*, 273–288.
Schäfer, R., Kramer, R., Zillig, W., & Cudny, H. (1973) *Eur. J. Biochem. 40*, 367–373.
Seidman, S., Surzycki, S. J., DeLorbe, W., & Gussin, G. N. (1979) *Biochemistry 18*, 3363–3371.
Smith, S. S., & Braun, R. (1978) *Eur. J. Biochem. 82*, 309–320.
Southern, E. M. (1975) *J. Mol. Biol. 98*, 503–517.
Surzycki, S. J., Surzycki, J. A., & Gussin, G. N. (1976) *Mol. Gen. Genet. 143*, 167–175.
Walter, G., Zillig, W., Palm, P., & Fuchs, E. (1967) *Eur. J. Biochem. 3*, 194–201.
Williams, R. C., & Chamberlin, M. J. (1977) *Proc. Natl. Acad. Sci. U.S.A. 74*, 3740–3744.

On the Structure and Conformational Dynamics of Yeast Phenylalanine-Accepting Transfer Ribonucleic Acid in Solution†

Måns Ehrenberg,* Rudolf Rigler,* and Wolfgang Wintermeyer

ABSTRACT: The solution structure of yeast $tRNA^{Phe}$ was investigated by using ethidium as a fluorescent probe in the D loop and the anticodon loop. For this purpose the dihydrouracils in position 16/17 and wybutine in position 37 were substituted by ethidium. The lifetimes and the time-dependent anisotropy of ethidium fluorescence were measured by pulsed nanosecond fluorometry. The kinetics of the transitions between different states of the $tRNA^{Phe}_{Etd}$ derivatives were determined by chemical relaxation measurements. It was found that the ethidium label irrespective of its position exhibits three different states called T_1, T_2 and T_3 characterized by lifetimes τ_1 = 30 ns, τ_2 = 12 ns, and τ_3 = 3 ns. The lifetime differences are due to different accessibilities of ethidium for solvent quenching in the three states. Thus, there are three different defined structural environments of the ethidium in both the anticodon and the D loop. The distribution of the three states was measured as a function of Mg^{2+} concentration and temperature; it was found that state T_3 is favored over states T_2 and T_1 by both increasing Mg^{2+} concentration and increasing temperature. The chemical relaxation kinetics exhibit a fast transition between T_1 and T_2 (10–100 ms) and a slow transition between T_2 and T_3 (100–1000 ms). The rates of both transitions depend likewise on Mg^{2+} concentration and temperature. The equilibrium and kinetic data clearly show the presence of strong and weak interactions between Mg^{2+} and tRNA. A cooperative model accounting for this behavior is developed. The ethidium probe behaves identically when located in different regions of the tRNA regarding both its distribution of states and its transition kinetics. This suggests that the different spectroscopic states report different conformations of the tRNA structure. The dependence of the three states on Mg^{2+} and spermine indicates that conformation T_3 is closely related to or identical with the crystal structure. The rotational diffusion constants indicate that of all three states T_3 is most extended while T_2 is most compact. The thermodynamic analysis reveals that the strongly bound Mg^{2+} ions reduce both the activation entropy and enthalpy of all transitions. The weakly bound Mg^{2+} ions increase both the activation enthalpy and entropy of the slow transition between T_2 and T_3. It is suggested that the breaking of several intramolecular bonds, e.g., hydrogen bonds, is involved in this transition.

A substantial amount of information has been accumulated from the crystal structure of yeast $tRNA^{Phe}$ regarding the role of conserved regions of tRNA in the folding of a conformation of tRNA which could be crystallized in the presence of Mg^{2+} and spermine (Kim et al., 1971; Ladner et al., 1972). Although a detailed picture of the tertiary folding of $tRNA^{Phe}$ (Kim et al., 1974; Ladner et al., 1975) now is available, the information regarding the functional role of this tRNA structure is very limited.

Studies of the interaction of $tRNA^{Phe}$ with ribosomal RNA and ribosomes suggest that the TΨCG sequence, which in the crystal structure is hydrogen-bonded to the D loop, can become available for hydrogen bonding (Erdmann et al., 1973; Richter et al., 1974; Schwarz et al., 1976). Thus, it is not unreasonable to assume the existence of tRNA conformations in solution which are different from the crystal structure.

The presence of such conformations is indicated by a variety of observations. Experiments in which the binding of oligonucleotides to tRNA was investigated indicate interactions between oligonucleotides and complementary sequences in the D loop (Uhlenbeck, 1972; Cameron & Uhlenbeck, 1973) as well as in the the anticodon loop (Uhlenbeck, 1972; Eisinger & Spahr, 1973) which are not expected to take place if the crystal structure prevails in solution.

The results of degradation studies of tRNA with exonucleases have been explained by the existence of at least two tRNA conformations which differ at or near the 3′ end (Thang et al., 1971) and at the 5′ end (Hänggi et al., 1970). Similar conclusions have been drawn from experiments in which the translational diffusion of $tRNA^{Phe}$ was investigated under various ionic conditions (Olson et al., 1976). NMR experiments have revealed two magnetic environments of the nucleoside T in $tRNA^{Phe}_{yeast}$ (Kan et al., 1977), indicating two

† From the Department of Medical Biophysics, Karolinska Institutet, Stockholm, Sweden (M.E. and R.R.), and the Institut für Physiologische Chemie, Physikalische Biochemie und Zellbiologie, der Universität München, München, West Germany (W.W.). *Received February 21, 1979.* This investigation was supported by grants from the Swedish Cancer Society, the Swedish Natural Science Research Council, the K. and A. Wallenberg foundation, and Deutsche Forschungsgemeinschaft (SFS 51).

0006-2960/79/0418-4588$01.00/0

conformations of the TΨCG loop under native conditions. Two different solution structures of tRNA^{Val} have been deduced from the observation of split methyl resonances both in the anticodon loop and in the TΨCG loop (Reid, 1977).

In continuation of previous reports on the existence of two spectroscopically different states of tRNA^{Phe} (Ehrenberg, 1975; Rigler & Ehrenberg, 1976; Rigler et al., 1977) visualized by the fluorescence of ethidium in positions 16/17 or 37 of tRNA^{Phe}, we now present a more detailed study concerning the presence of different conformational states of yeast tRNA^{Phe} in solution.

Materials and Methods

Materials

Ethidium-Labeled tRNAs and tRNA Fragments. tRNA^{Phe} was isolated from brewer's yeast tRNA (Boehringer, Mannheim) (Wintermeyer & Zachau, 1975a) and accepted 1.3–1.5 nmol of Phe per A_{260} unit. tRNA^{Phe} ethidium derivatives were prepared by replacing wybutine (tRNA$^{Phe}_{Etd37}$) or dihydrouracil (tRNA$^{Phe}_{Etd16/17}$) with ethidium and were isolated by column chromatography on RPC 5 (Wintermeyer & Zachau, 1971, 1974, 1979; Wintermeyer et al., 1979a). Two species of tRNA$^{Phe}_{Etd37}$ were separated, which were designated B and C; they probably represent the products of the condensation of the 7- and the 2-amino groups of ethidium, respectively, with the ribosylic aldehyde group in tRNA$^{Phe}_{-YWye}$ (Wintermeyer & Zachau, 1979). tRNA$^{Phe}_{Etd16/17}$ was shown to consist of a mixture of tRNA$^{Phe}_{Etd16}$ (38%), tRNA$^{Phe}_{Etd17}$ (52%), and tRNA$^{Phe}_{Etd16+17}$ (10%); 10–15% of the molecules contain ethidium also at the m^{7}G position (Wintermeyer & Zachau, 1979). The latter does not contribute significantly to the fluorescence signal of tRNA$^{Phe}_{Etd16/17}$ since it has a rather low quantum yield of fluorescence (unpublished experiments). All tRNA^{Phe} ethidium derivatives were chargeable by phenylalanyl-tRNA synthetase from yeast (1.1–1.3 nmol of Phe per A_{260} unit) and *Escherichia coli* (Wintermeyer & Zachau, 1971, 1979). They have been shown to be active in the ribosomal systems from yeast (Robertson et al., 1977) and *E. coli* (Wintermeyer & Zachau, 1975b).

The ethidium-containing dodecanucleotides Phe-31–42 (Etd-37B) and Phe-31–42 (Etd-37C) were isolated from T_1 RNase digestion mixtures of tRNA$^{Phe}_{Etd37B}$ and tRNA$^{Phe}_{Etd37C}$, respectively, by DEAE-cellulose chromatography. The homogeneity was established by electrophoresis on polyacrylamide gels (Wintermeyer & Zachau, 1979).

The ethidium labeled half-molecule Phe-1–36 (Etd-16/17) was prepared from Phe-1–36 (Thiebe & Zachau, 1969) following the procedure described for the preparation of tRNA$^{Phe}_{Etd16/17}$ (Wintermeyer et al., 1979b). T_1 RNase digestion of the labeled material yielded the same ethidium-containing oligonucleotides from the D region did as tRNA$^{Phe}_{Etd16/17}$ (Wintermeyer & Zachau, 1979), thus proving the designation of the fragment.

Reagents. Tris (Trizma) was obtained from Sigma Chemical Co., St. Louis, MO, and from E. Merck, Darmstadt, West Germany, wherefrom all other chemicals (analytical grade) were purchased.

Sample Preparation and Measuring Conditions. In order to remove divalent cations, we dialyzed the tRNAs and tRNA fragments (at 4 °C) against two changes (4 h) each of the following buffers: 10 mM Tris-HCl, pH 7.5, 1 M KCl, and 5 mM EDTA; 10 mM Tris-HCl, pH 7.5, and 5 mM EDTA; 10 mM Tris-HCl, pH 7.5, 0.1 M KCl, and 0.1 mM EDTA. According to atomic absorption measurements, the dialyzed samples contained less than one Mg^{2+} ion per tRNA molecule. All experiments were performed in the last dialysis buffer containing varying amounts of $MgCl_2$.

Methods

Fluorescence Titrations. Fluorescence titrations were performed in a laboratory-built instrument consisting of a stabilized 200-W high-pressure xenon lamp, Zeiss M_4QIII prism monchromators for selecting the excitation and emission wavelengths, and a photon counter (SSR 1140 Quantum photometer) as the detection unit. The fluorescence was excited at 510 nm and measured at 590 nm. Titrations were performed by adding aliquots of Mg^{2+} to ethidium-labeled tRNA^{Phe} without changing the concentration of tRNA.

Measurements of Fluorescence Lifetimes and Rotational Relaxation Times. Fluorescence lifetimes as well as rotational relaxation times observed after excitation with a short pulse of polarized light were determined in an instrument constructed in this laboratory (Rigler & Ehrenberg, 1976). The excitation wavelength was 510 nm and the emission was passed through an OG 590 cutoff filter (Schott & Gen., West Germany).

Measurements of Chemical Relaxation Times. The measurements were performed in a temperature-jump apparatus described previously (Rigler et al., 1974). The fluorescence was excited at 546 nm and measured after passing through an OG 590 cutoff filter.

Data Evaluation. The polarized and unpolarized components of the fluorescence emission were fitted to theoretical models convoluted with the system response according to an algorithm of Grinvald & Steinberg (1974). The model fitting was performed with a program for nonlinear regression (Meeter, 1964) based on an algorithm of Marquardt (1963). The minimization program was modified so that maximum likelihood estimates of the parameters were obtained (Rigler & Ehrenberg, 1976). The χ^2 values mentioned in the text and given in Tables I–IV are defined according to

$$\chi^2 = \frac{1}{N - C}\sum_{i=1}^{N}\frac{(e_i - f_i)^2}{f_i}$$

e_i is the measured emission intensity averaged in channel i, and f_i is its theoretically predicted value. C is the number of parameters, and N is the number of observables. The sum of squares is a χ^2-distributed stochastic variable with expectation value 1 and $N - C$ degrees of freedom. In Tables I and IV N is 400 and in Tables II and III N is 1000.

The photon-counting technique offers a theoretical knowledge of the accuracy in each point along an experimental curve (Rigler & Ehrenberg, 1976) as long as systematic errors are negligible in relation to photon noise. This experimental condition, which allows stringent statistical analysis of parameter errors and in model discrimination, was achieved through a device for sequential detection of the excitation pulse, the unpolarized fluorescence response, and the polarized emission (Rigler & Ehrenberg, 1976).

Estimates of chemical relaxation times and amplitudes in the temperature-jump experiments were also obtained with nonlinear regression. Here, starting values for the parameters were obtained by superimposing the measured signal on the oscilloscope with exponential functions generated by an analogue simulator (Rigler et al., 1977). Errors of the estimated parameters were obtained from a t test (Meeter, 1964).

Results

Fluorescence Titrations. The steady-state fluorescence for the two isomers tRNA$^{Phe}_{Etd37C}$ and tRNA$^{Phe}_{Etd37B}$ was recorded

Table I: Inverse Fluorescence Lifetimes $1/\tau_i$ for $tRNA^{Phe}_{Etd16/17}$ at 10 °C

species	$[MgCl_2]$ (mM)	$1/\tau_1 \times 10^2$ (ns^{-1})	$\sigma \times 10^2$ (ns^{-1})	$1/\tau_2 \times 10^2$ (ns^{-1})	$\sigma \times 10^2$ (ns^{-1})	$1/\tau_3 \times 10^2$ (ns^{-1})	$\sigma \times 10^2$ (ns^{-1})	χ^2
$tRNA^{Phe}_{Etd16/17}$	0.0	3.66	0.057	6.97	0.48	21.52	3.03	1.13
	0.042	3.64	0.042	6.82	0.29	21.43	1.49	1.09
	0.090	3.72	0.060	7.13	0.55	21.50	2.35	1.14
	0.184	3.65	0.082	6.72	0.51	21.12	2.17	0.99
	0.374	3.68	0.056	7.70	0.40	23.05	1.69	1.08
	0.847	3.69	0.058	7.60	0.50	25.96	2.76	1.04
	1.80	3.80	0.034	8.43	0.38	30.75	2.50	1.09
	4.64	3.71	0.061	7.64	0.46	28.00	1.92	0.96
	9.37	3.75	0.051	8.47	0.42	23.59	2.47	1.10
	18.8	3.78	0.028	8.90	0.23	36.95	1.46	1.08
	47.3	3.68	0.066	8.13	0.35	35.92	1.94	1.03
	84.6	3.74	0.032	8.30	0.24	35.16	1.35	1.04

Table II: Inverse Fluorescence Lifetimes $1/\tau_i$ and Quenching Rates k_i According to Equation 3 for $tRNA^{Phe}_{Etd37B}$ at 10 °C and for $tRNA^{Phe}_{Etd16/17}$ at 10 and 24 °C[a]

species	temp (°C)	$1/\tau_1 \times 10^2$ (ns^{-1})	$1/\tau_2^0 \times 10^2$ (ns^{-1})	$k_2 \times 10^{-7}$ (M^{-1} s^{-1})	$1/\tau_3^0 \times 10^2$ (ns^{-1})	$k_3 \times 10^{-7}$ (M^{-1} s^{-1})	χ^2
$tRNA^{Phe}_{Etd37B}$	10	3.29 ± 0.02	7.2 ± 0.1	4.3 ± 1.2	21.4 ± 0.6	37.3 ± 6.9	1.14
$tRNA^{Phe}_{Etd16/17}$	10	3.81 ± 0.02	8.5 ± 0.2	6.6 ± 2.8	30.7 ± 1.3	116 ± 32	1.10
$tRNA^{Phe}_{Etd16/17}$	24	3.87 ± 0.01	8.6 ± 0.1	8.7 ± 1.8	33.4 ± 0.7	60 ± 15	1.03

[a] The parameters were obtained in a joint evaluation of the I_m vectors at different Mg^{2+} concentrations with the lifetimes related according to eq 3. The quenching rate for τ_1 was put to zero [τ_1 was found to be independent of the concentration of $MgCl_2$ (Table I)].

Table III: Inverse Rotational Relaxation Time $1/\tau_R$, Molecular Volume V, and Translational Diffusion Constant D for $tRNA^{Phe}_{Etd16/17}$ at 24 °C[a]

species	$[MgCl_2]$ (mM)	$1/\tau_R \times 10^2$ (ns^{-1})	$V \times 10^{-3}$ (Å^3)	$D \times 10^7$ (cm^2 s^{-1})	χ^2
$tRNA^{Phe}_{Etd16/17}$	0.0	4.74 ± 0.09	94.55	8.41	1.16
	0.042	4.61 ± 0.16	97.22	8.34	1.24
	0.089	4.40 ± 0.15	101.9	8.20	1.31
	0.183	4.77 ± 0.16	93.96	8.43	1.09
	0.372	4.68 ± 0.11	95.76	8.38	1.38
	0.844	4.59 ± 0.18	97.65	8.32	0.99
	1.79	4.41 ± 0.21	101.6	8.21	1.14
	4.62	3.68 ± 0.18	121.8	7.73	1.10
	9.34	3.36 ± 0.17	133.4	7.50	1.17
	18.8	3.67 ± 0.18	122.1	7.72	1.81
	47.1	4.31 ± 0.29	104.0	8.15	1.18
	94.3	3.60 ± 0.34	121.5	7.74	1.09

[a] V and D were obtained from the relations $1/\tau_R = kT/(V\eta)$ and $D = kT/(6\pi\eta r)$ assuming a rigid spherical particle (k is Boltzmann's constant, T is absolute temperature, r is molecular radius, and η is viscosity of the solvent).

as a function of $MgCl_2$ concentration at various temperatures. The results at 10 °C are displayed in Figure 1A. The emission intensity decreases for both derivatives to about 50% of its starting value. The fluorescence has a marked decrease at low $MgCl_2$ concentrations, followed by a further decrease at higher $MgCl_2$ concentrations. The intact $tRNA^{Phe}_{Etd37}$ molecule is required for this behavior, as can be seen from $MgCl_2$ titrations with the fragments Phe-31–42 (Etd-37C) and Phe-31–42 (Etd-37B) at the same temperature (Figure 1A).

Similarly the fluorescence emission of $tRNA^{Phe}_{Etd16/17}$ decreases when the concentration of $MgCl_2$ increases (Figure 1B). For fragment Phe-1–36 (Etd-16/17) the decrease in fluorescence intensity is small (Figure 1B).

Fluorescence Lifetimes. The time-resolved emission of $tRNA^{Phe}_{Etd37C}$ could be described by two fluorescence lifetimes at 10 °C (Rigler et al., 1977). At higher temperatures a third component in the fluorescence decay had to be introduced as judged from χ^2 test and residual plots.

The unpolarized fluorescence component $I_m(t)$ measured in the magic angle was described by

$$I_m(t) = A_1 e^{-t/\tau_1} + A_2 e^{-t/\tau_2} \quad (1)$$

The lifetime τ_1 was estimated as 30 ns and τ_2 was estimated as 10 ns. Changes in $MgCl_2$ concentration and in temperature influenced the amplitudes A_1 and A_2 but not the lifetimes τ_1 and τ_2. The normalized amplitudes $A_1/(A_1 + A_2)$ and $A_2/(A_1 + A_2)$ at different Mg^{2+} concentrations are shown in Figure 2A.

For $tRNA^{Phe}_{Etd37B}$ and $tRNA^{Phe}_{Etd16/17}$ the lifetime spectra were described by three lifetimes in the temperature range 10–35 °C and in the concentration interval 0–100 mM Mg^{2+}:

$$I_m(t) = \sum_{i=1}^{3} A_i e^{-t/\tau_i} \quad (2)$$

Table IV: Inverse Rotational Relaxation Time $1/\tau_R$ and Amplitude R, Molecular Volume V, and Translational Diffusion Constant D for the Conformations T_1, T_2, and T_3 for $tRNA^{Phe}_{Etd37B}$ and $tRNA^{Phe}_{Etd16/17}$ at 24 °C[a]

species	conformation	$1/\tau_R \times 10^2$ (ns^{-1})	R	$V \times 10^{-3}$ (Å^3)	$D \times 10^7$ (cm^2 s^{-1})	χ^2
$tRNA^{Phe}_{Etd37B}$	T_1	3.54 ± 0.46	0.415 ± 0.062	126.6	7.63	
	T_2	5.32 ± 0.26	0.605 ± 0.031	84.25	8.74	1.23
	T_3	1.78 ± 0.55	0.519 ± 0.014	251.8	6.07	
$tRNA^{Phe}_{Etd16/17}$	T_1	4.68 ± 0.26	0.627 ± 0.021	95.77	8.38	
	T_2	6.19 ± 0.47	0.557 ± 0.043	72.41	9.20	1.13
	T_3	5.67 ± 4.4	0.223 ± 0.030	79.05	8.93	

[a] V and D were obtained as described in Table III.

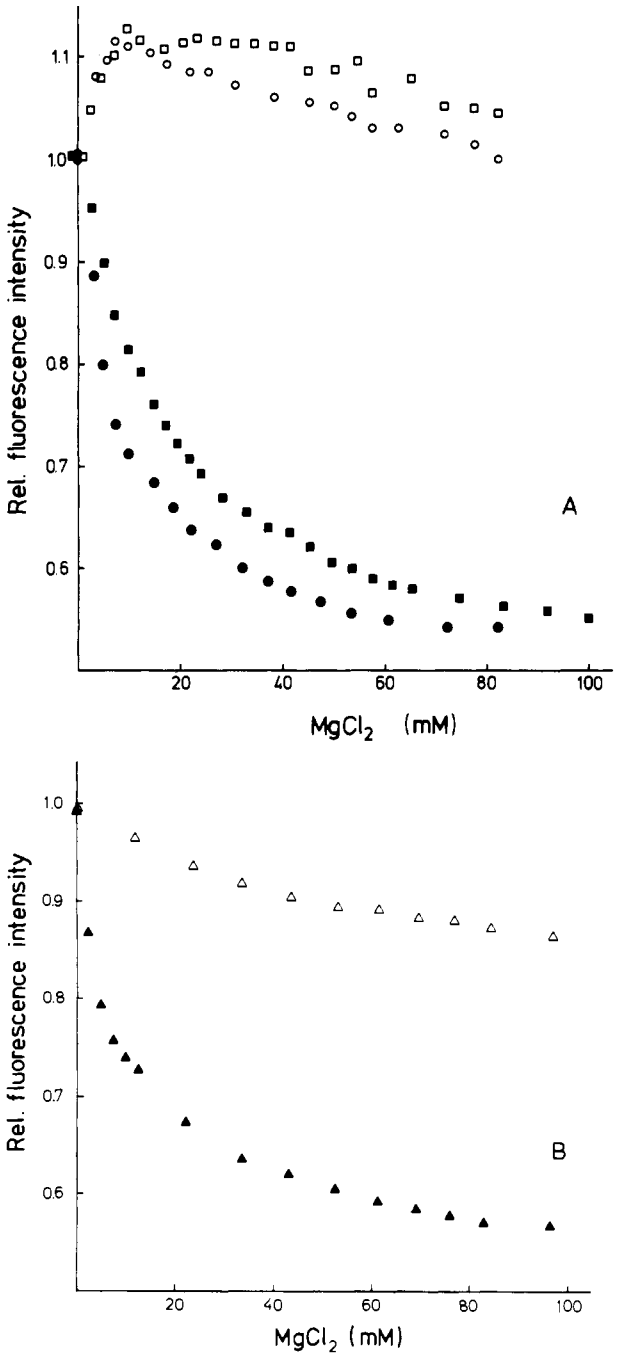

FIGURE 1: (A) Fluorescence intensity of tRNA$^{Phe}_{Etd37B}$ (●) and tRNA$^{Phe}_{Etd37C}$ (■) and of the corresponding fragments 31–42 (Etd-37) (open symbols) at different $MgCl_2$ concentrations in Tris buffer at 10 °C. (B) The fluorescence intensity of tRNA$^{Phe}_{Etd16/17}$ (▲) and of fragment 1–36 (Etd-16/17) (△) at different $MgCl_2$ concentrations at 10 °C.

For tRNA$^{Phe}_{Etd16/17}$ the inverse lifetimes $1/\tau_i$ (i = 1, 2, and 3) are given as functions of the Mg^{2+} concentration at 10 °C in Table I.

The longest fluorescence lifetime is constant. The intermediate lifetime decreases moderately and the shortest decreases substantially when the concentration of $MgCl_2$ is increased. The longest lifetime τ_1, which is about 30 ns, has a value similar to what is found for ethidium bromide intercalated in DNA (Tao et al., 1970).

According to a proposal of Olmsted & Kearns (1977), the long lifetime is due to shielding of the ethidium from the solvent. The appearance of an intermediate and a short lifetime indicates that there are two other arrangements in which the dye is more exposed.

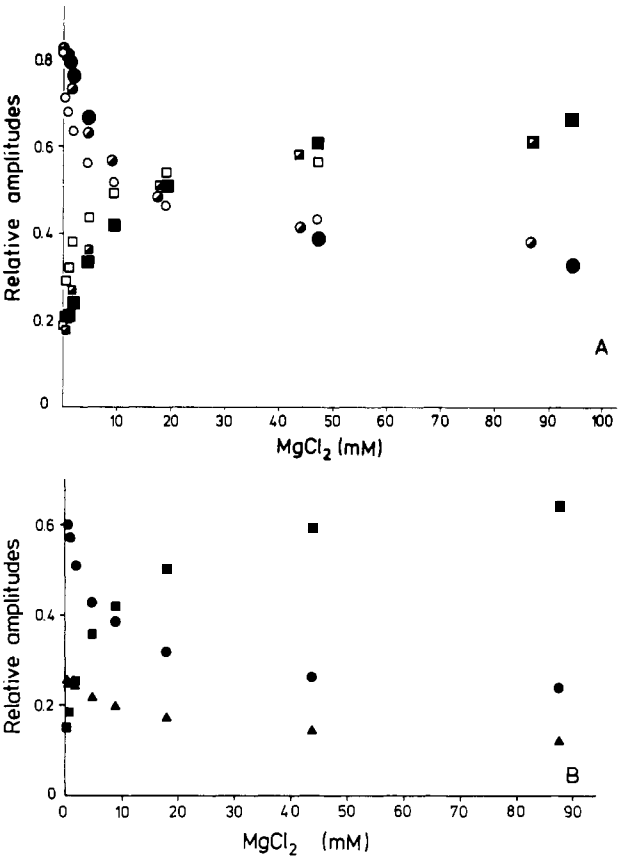

FIGURE 2: (A) Normalized amplitudes a_1 (●) and a_2 (■) for tRNA$^{Phe}_{Etd37C}$. With probabilities of T_1 and T_2 added for tRNA$^{Phe}_{Etd16/17}$ [$a_1 + a_2$ (○); a_3 (□)] and for tRNA$^{Phe}_{Etd37B}$ [$a_1 + a_2$ (◑); a_3 (◪)] at 10 °C. (B) Normalized amplitudes a_1 (▲), a_2 (●), and a_3 (■) for tRNA$^{Phe}_{Etd37B}$ at 10 °C.

The drifts in the shortest and intermediate lifetimes, which are observed when the $MgCl_2$ concentration is raised (Table I), could result from collisional quenching by either Mg^{2+} or Cl^- ions. As expected, this process is effective only for the states T_2 and T_3 which are accessible for both solvent and solute molecules.

According to this assumption the Mg^{2+} dependence of the shorter lifetimes is

$$1/\tau_i = 1/\tau_i^0 + k_i[MgCl_2]; \qquad i = 1 \text{ and } 2 \qquad (3)$$

$1/\tau_i^0$ as well as the quenching rates k_i are given in Table II for tRNA$^{Phe}_{Etd37B}$ at 10 °C and for tRNA$^{Phe}_{Etd16/17}$ at 10 and 24 °C.

The relative amplitudes for tRNA$^{Phe}_{Etd37B}$ at 10 °C are shown in Figure 2B, and the relative amplitudes for tRNA$^{Phe}_{Etd16/17}$ at 10 and 24 °C are displayed in parts A and B of Figure 3 at different Mg^{2+} concentrations.

The amplitude A_i is related to the state T_i with concentration $[T_i]$ identified by its lifetime τ_i by the relation (Rigler & Ehrenberg, 1973, 1976)

$$A_i = [T_i]\epsilon_i q_i^e; \qquad i = 1, 2, \text{ and } 3 \qquad (4)$$

where ϵ_i is the extinction coefficient and q_i^e is the emission rate of T_i. If the product $\epsilon_i q_i^e$ is the same for all A_i, the relative amplitudes in Figures 2 and 3 directly describe the $[Mg^{2+}]$-dependent probability of the state T_i. If the lifetimes of the states T_1, T_2, and T_3 are determined by their different proton transfer rates to the solvent, then their emission rates q^e are the same (Olmsted & Kearns, 1977). Furthermore, absorption spectra measured at different Mg^{2+} concentrations

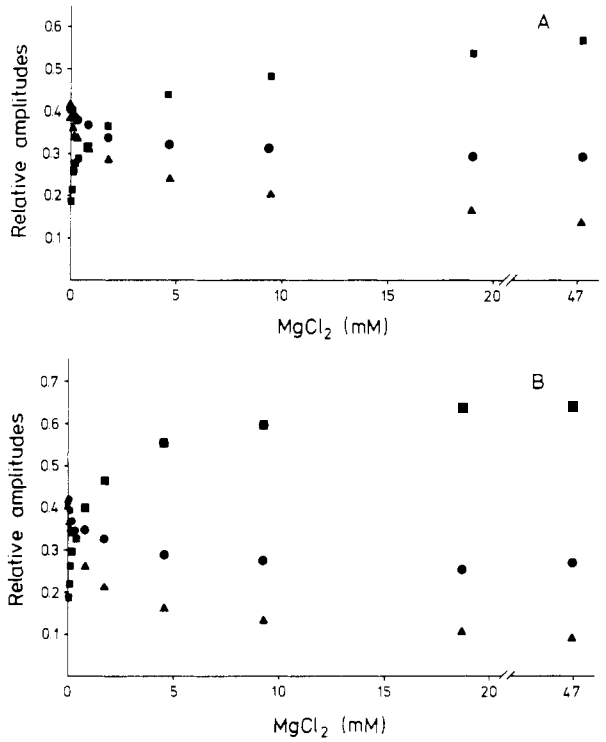

FIGURE 3: Dependence of the normalized amplitudes a_1 (▲), a_2 (●), and a_3 (■) of $tRNA^{Phe}_{Etd16/17}$ on the concentration of $MgCl_2$ at 10 (A) and 24 °C (B).

for the tRNA ethidium derivative have an isosbestic point near 510 nm, the excitation wavelength in all pulsed measurements. Therefore, it is assumed that the relative amplitude $A_i/\sum_j A_j$ is a close approximation of the probability of the state T_i.

If the probabilities for T_1 and T_2 of $tRNA^{Phe}_{Etd37B}$ (Figure 2B) and of $tRNA^{Phe}_{Etd16/17}$ (Figure 3A) are added, amplitude spectra similar to that of $tRNA^{Phe}_{Etd37C}$ (Figure 2A) are obtained. This suggests that the label in $tRNA^{Phe}_{Etd37C}$ has three states which behave identically as in $tRNA^{Phe}_{Etd37B}$ and in $tRNA^{Phe}_{Etd16/17}$ but where the fluorescence lifetimes of T_1 and T_2 are too close to be resolved.

The steady-state fluorescence titrations in Figure 1 can now be understood. Assuming that $\epsilon_i q_i^e$ is the same for all three species of ethidium, the steady-state fluorescence intensity is obtained from eq 2 and 4 by time averaging:

$$I(c) = \text{constant} \cdot \sum_{i=1}^{3} [T_i] \epsilon_i q_i^e \tau_i \qquad (5)$$

where c is the Mg^{2+} concentration. The concentration of T_1 decreases when Mg^{2+} is added (Figures 2B and 3A). Since T_1 has the longest fluorescence lifetime, it follows from eq 5 that the steady-state fluorescence intensity decreases too (Figure 1). The Mg^{2+} binding curves are biphasic (Figure 3); apparently there are strong Mg^{2+} binding sites in the tRNA molecule which saturate at $MgCl_2$ concentrations below 1 mM and weak ones which saturate only at about 20 mM $MgCl_2$.

Rotational Relaxation Times. The polarized component of the fluorescence emission from a labeled macromolecule contains information about the hydrodynamic properties of the carrier molecule [e.g., Chuang & Eisenthal (1972), Ehrenberg & Rigler (1972), and Belford et al. (1972)]. The polarized component parallel with the polarization vector of the exciting beam was interpreted according to [cf. Chuang & Eisenthal (1972) and Ehrenberg & Rigler (1972)]

$$I_{\parallel}(t) = \sum_{i=1}^{3} (1 + Re^{-t/\tau_R}) A_i e^{-t/\tau_i} \qquad (6)$$

$R = 2r$, where r is the limiting anisotropy at infinitely high viscosity in steady-state measurements. The amplitudes A_i and fluorescence lifetimes τ_i were taken from evaluations of the corresponding depolarized emission vector $I_m(t)$. The Mg^{2+} dependence of the inverse rotational relaxation time, $1/\tau_R$, as well as of the molecular volume V and the translational diffusion constant D for $tRNA^{Phe}_{Etd16/17}$ at 24 °C are shown in Table III.

An increasing concentration of $MgCl_2$ leads to increased rotational tumbling times, i.e., the overall motion of the molecule is slowed down. This may be interpreted in terms of a less compact structure at high Mg^{2+} concentration.

If the spectroscopic states T_1, T_2, and T_3 correspond to three conformations of the tRNA molecule with different hydrodynamic properties, then the rotational relaxation times evaluated from eq 6 are combinations of the separate rotations of T_1, T_2, and T_3. We have evaluated such a model by ascribing one rotational relaxation time $\tau_{R(i)}$ and one anisotropy amplitude R_i to each lifetime τ_i according to

$$I_{\parallel}(t) = \sum_{i=1}^{3} A_i e^{-t/\tau_i} (1 + R_i e^{-t/\tau_{R(i)}}) \qquad (7)$$

The polarized fluorescence vectors $I_{\parallel}(t)$ measured at different Mg^{2+} concentrations were jointly evaluated to obtain the six parameters R_i and τ_i (i = 1, 2, and 3) for $tRNA^{Phe}_{Etd16/17}$ at 10 and 24 °C and for $tRNA^{Phe}_{Etd37B}$ at 24 °C. The joint evaluation of several experiments with different amplitude factors, A_i, makes the determination of the parameters unique and gives a precision high enough to resolve some of the parameters in eq 7.

Rotational relaxation times and anisotropy amplitudes are shown in Table IV as well as molecular volumes and translational diffusion constants for the states T_1, T_2, and T_3. T_2 has a significantly shorter rotational relaxation time than T_1. As expected, since τ_3 is so short, the estimates for $\tau_{R(3)}$ have a low accuracy. For $tRNA^{Phe}_{Etd37B}$, where the best estimate for $\tau_{R(3)}$ is obtained, $\tau_{R(3)}$ is longer than $\tau_{R(2)}$ and $\tau_{R(1)}$.

Chemical Kinetics and Thermodynamic Relations. The relaxation curves for $tRNA^{Phe}_{Etd37C}$ obtained with a temperature jump (ΔT = 7 °C) to 10 °C showed one chemical relaxation time in the Mg^{2+} concentration range 0–100 mM (Rigler et al., 1977). Reciprocal relaxation times $1/\tau_{CH}$ and relative relaxation amplitudes $\delta I(0)/I$ were evaluated according to

$$\frac{\delta I(t)}{I} = \frac{\delta I(0)}{I} e^{-t/\tau_{CH(1)}} \qquad (8)$$

The relaxation time at zero $MgCl_2$ concentration is about 0.2 s and increases to a constant value of about 1 s when Mg^{2+} is added. The relative amplitude $\delta I(0)/I$ passes a maximum value of about 1% at 20 mM Mg^{2+} when the Mg^{2+} concentration is increased from 0 to 80 mM.

Relaxation curves for $tRNA^{Phe}_{Etd16/17}$ at 10 °C (Rigler et al., 1977) and for $tRNA^{Phe}_{Etd37B}$ (not shown) contain two relaxation times. Reciprocal relaxation times and relative amplitudes at different Mg^{2+} concentrations were evaluated according to

$$\frac{\delta I(t)}{I} = \frac{\delta I_1(0)}{I} e^{-t/\tau_{CH(1)}} + \frac{\delta I_2(0)}{I} e^{-t/\tau_{CH(2)}} \qquad (9)$$

For $tRNA^{Phe}_{Etd16/17}$ the two relaxation times observed after temperature jumps (ΔT = 7 °C) to 10, 17, and 24 °C are shown at different Mg^{2+} concentrations in Figure 4. Both relaxation times increase considerably when Mg^{2+} is added in low concentrations. At higher $MgCl_2$ concentration, $\tau_{CH(1)}$

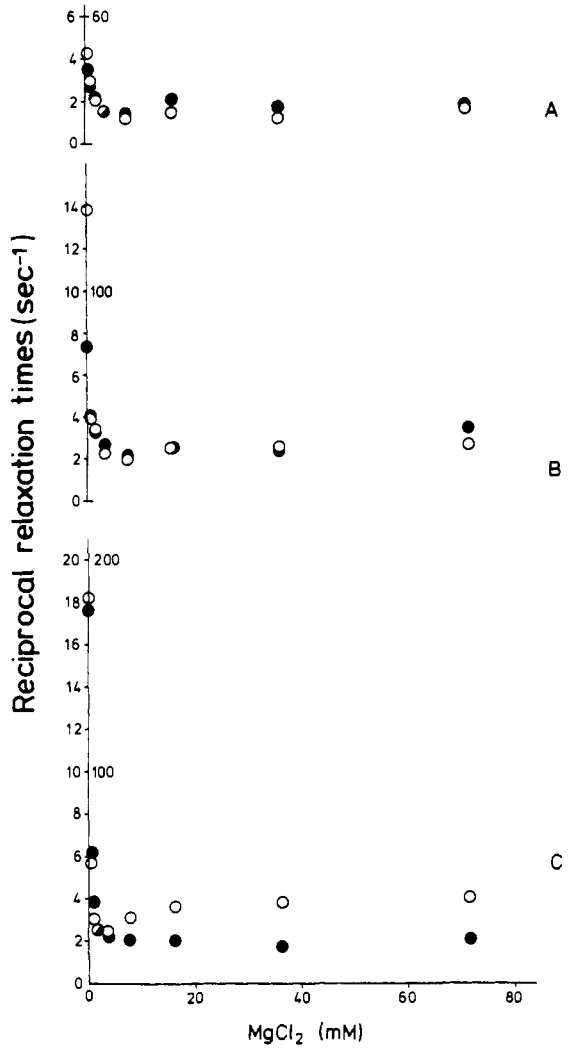

FIGURE 4: Dependence of the chemical relaxation times $1/\tau_{CH(1)}$ (○; left scale) and $1/\tau_{CH(2)}$ (●; right scale) of tRNA$^{Phe}_{Etd16/17}$ on the concentration of $MgCl_2$ for temperature jumps of 3–10 °C (A), 10–17 °C (B), and 17–24 °C (C).

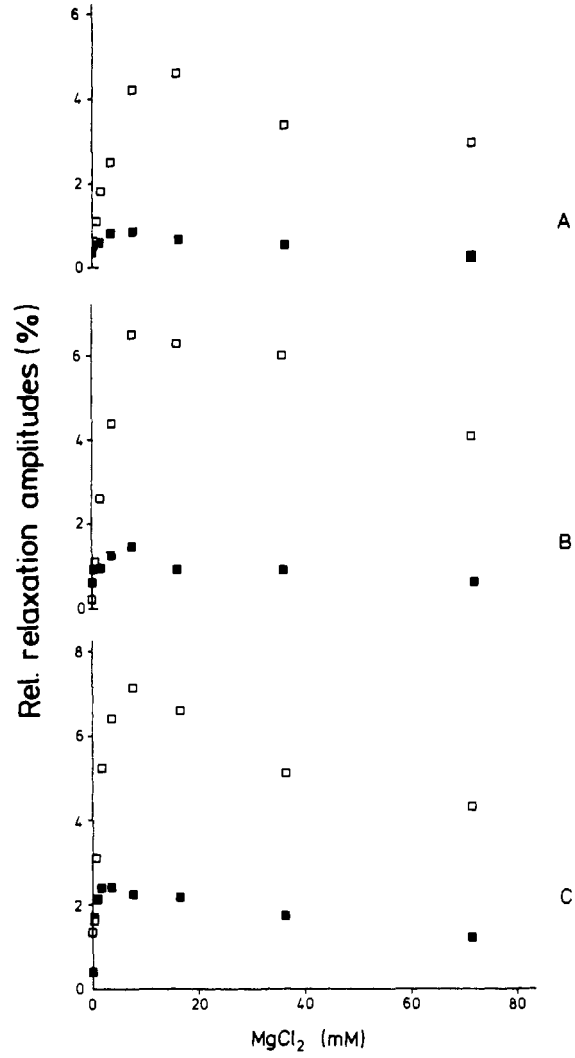

FIGURE 5: Dependence of the relative amplitudes $\Delta I_1/I$ (□) and $\Delta I_2/I$ (■) of tRNA$^{Phe}_{Etd16/17}$ on the concentration of $MgCl_2$ for temperature jumps of 3–10 °C (A), 10–17 °C (B), and 17–24 °C (C).

decreases so that is passes a maximum while $\tau_{CH(2)}$ remains approximately constant.

The corresponding relative amplitudes are shown in Figure 5. The amplitude of the longer relaxation time, $\delta I_1(0)/I$, passes a maximum value of about 6% at all three temperatures. The amplitude corresponding to the fast relaxation also has a maximum which ranges from 1% at 10 °C to 2.5% at 24 °C. The maxima of both amplitudes shift toward lower Mg^{2+} concentration when the temperature increases.

The two relaxation times and amplitudes of tRNA$^{Phe}_{Etd37B}$ behave as those of tRNA$^{Phe}_{Etd16/17}$. $\tau_{CH(1)}$ of both tRNAs behave as the single relaxation time detected for tRNA$^{Phe}_{Etd37C}$.

The amplitudes in Figure 3 contain for tRNA$^{Phe}_{Etd16/17}$ the Mg^{2+}-dependent equilibrium constants (cf. eq A2 and A15 of the Appendix)

$$R(c) = \frac{[T_2]}{[T_1]} = \frac{A_2}{A_1} = \frac{k_{12}(c)}{k_{21}(c)} \tag{10}$$

$$L(c) = \frac{[T_3]}{[T_1]} = \frac{A_3}{A_1} = \frac{k_{13}(c)}{k_{31}(c)} \tag{11}$$

The state T_1 is spectroscopically defined by a long fluorescence lifetime, the state T_2 is defined by an intermediate, and T_3 is defined by a short lifetime. The results from pulsed measurements can be combined with the chemical relaxation experiments, and all rate constants in the transitions between the three states of the label can be determined.

The fast chemical relaxation may occur between states T_1 and T_2

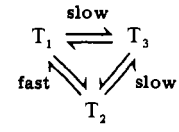

(12)

or between states T_2 and T_3

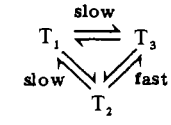

(13)

or finally between T_1 and T_3

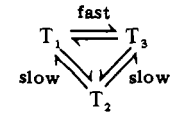

(14)

The amplitude spectra of the chemical relaxation experiments have been simulated (see Appendix) from equilibrium constants and quantum yields as determined in pulsed measurements at different temperatures. In this simulation, eq 12 gave the best correspondence between measured and

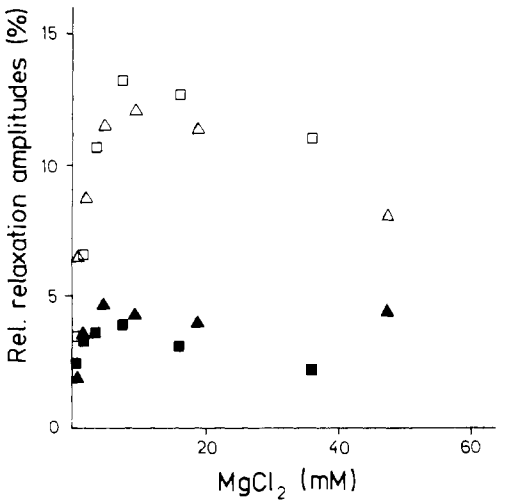

FIGURE 6: Comparison between the relative relaxation amplitudes $\Delta I_1/I$ (open symbols) and $\Delta I_2/I$ (closed symbols) of $tRNA^{Phe}_{Etd16/17}$ obtained from temperature jumps (□, ■) between 10 and 17 °C and between 17 and 24 °C (parts B and C of Figure 5) and calculated from amplitudes a_1, a_2, and a_3 obtained from the pulsed fluorescence decay experiments (△, ▲) at 10 and 24 °C (parts A and B of Figure 3).

calculated amplitudes (Figure 6).

The rate constants for eq A13

$$T_1 \underset{k_{21}(c)}{\overset{k_{12}(c)}{\rightleftharpoons}} T_2 \underset{k_{32}(c)}{\overset{k_{23}(c)}{\rightleftharpoons}} T_3$$

were evaluated with equilibrium constants $R(c)$ and $L(c)$ determined in pulsed experiments and chemical relaxation times from temperature-jump data according to eq A8 and A14.

All four rate constants decrease markedly as the concentration of Mg^{2+} is increased from 0 to about 1 mM (Figure 7A). At higher Mg^{2+} concentrations (1–80 mM), no large changes are seen for the transition $T_1 \rightleftharpoons T_2$. However, the transition $T_2 \rightleftharpoons T_3$ is markedly effected by weakly binding Mg^{2+} ions: the rate constant k_{23} increases with increasing Mg^{2+} concentration (Figure 7B).

These temperature effects can be formulated quantitatively in terms of activation entropies and activation enthalpies (Laidler, 1969). For the rate constant k_{ij} (cf. Appendix)

$$k_{ij}(c) = we^{-\Delta H^{\ddagger}_{ij}(c)/RT + \Delta S^{\ddagger}_{ij}(c)/R} \qquad (15)$$

In Figure 8A the activation entropies and enthalpies for the rate constants of transition $T_1 \rightleftharpoons T_2$ are shown, and in Figure 8B those for the transition $T_2 \rightleftharpoons T_3$ are shown. In the low Mg^{2+} concentration range both entropies and enthalpies for all four rate constants are markedly reduced when the magnesium concentration is increased. Further increase in concentration influences primarily the slow transition $T_2 \rightleftharpoons T_3$ so that the enthalpic reaction barrier gets higher again. This rate-decreasing effect is, however, compensated for by an increased activation entropy. Equations A26 and A28 (cf. Appendix) give a detailed description of how the four rate constants in eq A13 are influenced by Mg^{2+} ions.

Discussion

The structural properties of the $tRNA^{Phe}$ molecule have been visualized by using extrinsic probes. It is therefore important to assert that the native structure of the tRNA is not severely perturbed by the inserted dye molecules. All three ethidium derivatives ($tRNA^{Phe}_{Etd16/17}$, $tRNA^{Phe}_{Etd37B}$, and $tRNA^{Phe}_{Etd37C}$) used here are aminoacylated by the phenylalanyl-tRNA synthetases from both yeast and *E. coli* (Wintermeyer & Zachau, 1979), and they are active in the ribosomal systems

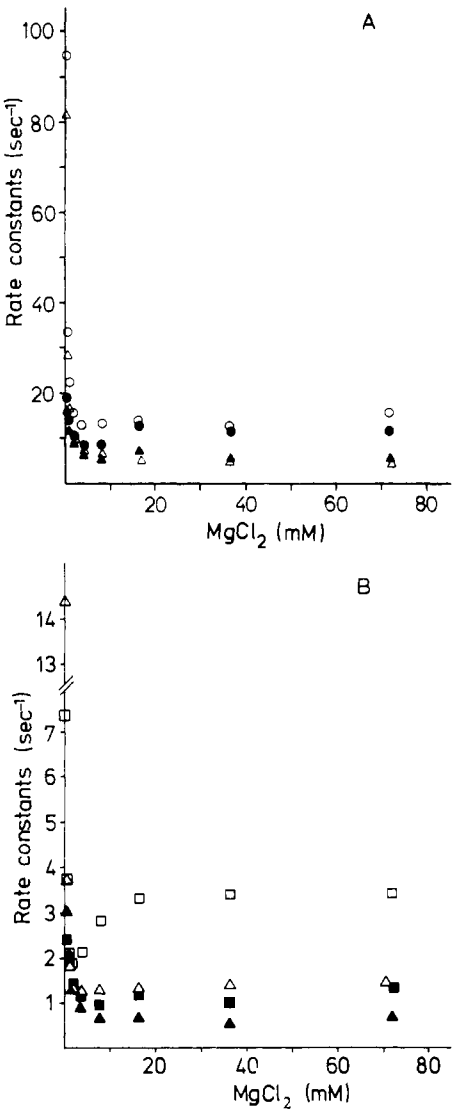

FIGURE 7: Dependence, for $tRNA^{Phe}_{Etd16/17}$, of (A) the rate constants k_{12} (●, ○) and k_{21} (▲, △) of the transition between T_1 and T_2 and (B) the rate constants k_{23} (■, □) and k_{32} (▲, △) of the transition between T_2 and T_3 on the concentration of $MgCl_2$ at two temperatures (10 °C, closed symbols; 24 °C, open symbols).

from both organisms (Robertson et al., 1977; Wintermeyer & Zachau, 1975b). From these data and from direct structural comparisons (Wintermeyer et al., 1979b), we conclude that the $tRNA^{Phe}_{Etd}$ derivatives do not differ from native $tRNA^{Phe}$ in essential features.

We have made our experiments under conditions where the tRNA is in its native state and is biologically active (Wintermeyer & Zachau, 1979). The dynamic picture of the tRNA structure which emerges from this work should therefore be of relevance for the biological functioning of the molecule.

Three Spectroscopic States of $tRNA^{Phe}_{Etd}$. An Interpretation. Three spectroscopic states of the ethidium label in the anticodon loop ($tRNA^{Phe}_{Etd37B}$) and in the D loop ($tRNA^{Phe}_{Etd16/17}$) have been identified in pulsed fluorescence measurements and with temperature-jump experiments.

The lifetimes and quenching rates (Table II) suggest that the label is most accessible to the solvent in state T_3 and least accessible in state T_1 and indicate differences in stacking between ethidium and neighboring nucleotides.

The observation that the ethidium label in both the D loop and the anticodon loop responds to Mg^{2+} concentration only in the intact tRNA structure (Figure 1) suggests that Mg^{2+}

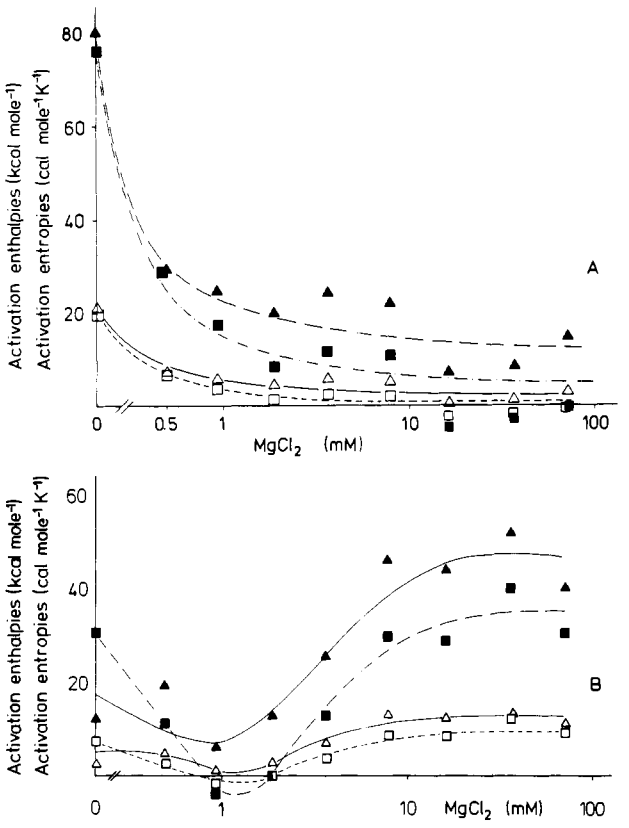

FIGURE 8: Activation enthalpies (open symbols) and activation entropies (closed symbols) for (A) the rate constants k_{12} (△, ▲) and k_{21} (□, ■) and for (B) the rate constants k_{23} (△, ▲) and k_{32} (□, ■).

influences the spectroscopic properties of the label by changes of the tRNA conformation rather than by a direct interaction.

It is remarkable to find similar distributions of T_1, T_2, and T_3 as well as the same transition kinetics irrespective of the position of the label. The most likely interpretation is that these states correspond to different conformations of the tRNA^{Phe} molecule, which force the dye into different positions in the nucleotide stack.

tRNA$_{Etd37C}^{Phe}$ exhibits only two states and only one chemical transition with the same $MgCl_2$ dependence as the slow relaxation time of tRNA$^{Phe}_{Etd37B}$ and tRNA$^{Phe}_{Etd16/17}$. This quantitative difference is probably related to similar and therefore nonseparable lifetimes for the states T_1 and T_2 in tRNA$^{Phe}_{Etd37C}$. Since in our case similar lifetimes lead to similar quantum yields, this would also lead to a vanishing of the temperature-jump amplitude for the fast transition. A prediction of this hypothesis is that, if the probabilities of the states T_1 and T_2 are added, all three derivatives should have identical amplitude spectra. The comparison in Figure 2A shows a striking similarity over the whole Mg^{2+} concentration range investigated.

The deviating behavior of tRNA$^{Phe}_{Etd37C}$ might also be explained by the existence of only two different tRNA conformations instead of three. Then the states T_1 and T_2 in tRNA$^{Phe}_{Etd16/17}$ and tRNA$^{Phe}_{Etd37B}$ would correspond to one tRNA structure where the label can have two isomeric states in contrast with tRNA$^{Phe}_{Etd37C}$ where in this conformation only one isomeric state is allowed.

The presence of different tRNA^{Phe} conformations is also supported by measurements of the wybutine fluorescence in unmodified yeast tRNA^{Phe}. The slow transition reported for the ethidium derivatives is also found for wybutine with the same Mg^{2+} concentration dependence of relaxation time and relative amplitude (Rigler et al., 1977). A conformational change around wybutine detected with the fluorescence temperature-jump technique has been reported by Urbanke & Maass (1978). However, since these experiments were done in the absence of Mg^{2+}, the observed effect probably does not reflect a transition of the native molecule and cannot be compared directly with the present results.

The results of our fluorescence experiments are in line with recent NMR results which indicate the presence of different conformations of the tRNA molecule in solution (Kan et al., 1977; Reid, 1977).

Binding of Magnesium Ions to tRNA^{Phe}. Our data indicate that tRNA^{Phe} in solution exists in at least two different tertiary structures. The Mg^{2+} concentration dependence of their equilibrium distributions is explained by a cooperative model (Appendix) which takes into account binding sites with different affinities.

In high salt concentration (0.1 M KCl, pH 7.5) there exist two types of Mg^{2+} binding sites. The equilibrium distributions for the three states of tRNA$^{Phe}_{Etd16/17}$ are shifted significantly at Mg^{2+} concentrations below 1 mM (Figure 3). Since we have no independent measure of the number of bound Mg^{2+} ions per tRNA molecule, it is difficult to separate the number of binding sites from the affinity of Mg^{2+}, and only approximate estimates of the association constants can be given. The strong sites have an affinity of about 10^4 M^{-1} and the weak sites have affinities of about 10^2 M^{-1} (cf. parts A and B of Figure 3), values which are compatible with those found for tRNA^{fMet} under similar ionic conditions (Stein & Crothers, 1976). Strong and weak Mg^{2+} binding sites have been reported previously for tRNA^{Phe} for the low ionic strength condition (Römer & Hach, 1975). The influence of the ionic strength on the electrostatic part of the binding potential has been discussed in detail (Walters et al., 1977; Leroy et al., 1977).

The kinetic investigations also reveal features of the Mg^{2+} binding which indicate at least two types of sites with different functional roles. There is a sharp increase in the chemical relaxation times (Figure 4) when the strong Mg^{2+} binding sites are occupied. The occupation of the weak sites leads to a moderate decrease in the slow chemical relaxation.

Fourier transform NMR studies of tRNA^{Phe} yield spin relaxation rates in saturation recovery experiments which are a direct measure of the solvent replacement for imino protons (Johnston & Redfield, 1977, 1978). These relaxation rates are of the same order of magnitude as the inverse chemical relaxation times observed by us and show a similar behavior when Mg^{2+} is added.

Information about the Mg^{2+} binding sites in tRNA^{Phe} has recently emerged from X-ray data (Holbrook et al., 1977; Jack et al., 1977; Quigley et al., 1978). The data suggest that the positions of Mg^{2+} ions in the D loop and the anticodon loop are rather close to the position of the ethidium label. Thus, a direct influence of Mg^{2+} on the lifetime distribution of ethidium is possible. However, we have observed that spermine affects the distribution of the ethidium states in the same manner as does Mg^{2+} (unpublished experiments) although the two spermine binding sites hitherto found in the crystal structure are far away from the positions of the ethidium label. This indicates that the mechanism by which both spermine and Mg^{2+} influence the fluorescence properties of the ethidium label is the same and consists of a ligand-induced global structural change of the tRNA molecule.

Thermodynamics of Mg^{2+} Binding to tRNA^{Phe}. The thermodynamic analysis also shows two different regions of Mg^{2+} interactions. The strongly bound Mg^{2+} ions decrease both activation enthalpies and entropies for all four rate

constants (Figure 8). The weakly bound Mg^{2+} ions increase both activation enthalpy and entropy for the slow transition. This indicates that the strong sites are different from the weak ones and that the ordering of the $tRNA^{Phe}$ structure by Mg^{2+} ions proceeds in two thermodynamically different ways. Our thermodynamic data show that the slow conformational transition induced by weakly binding Mg^{2+} ions is connected with a high activation barrier (Figure 8B). They support the idea that several intramolecular bonds, e.g., hydrogen bonds, have to be broken in this transition and suggest a substantial change of the tRNA conformation.

Rotational Brownian Motion of $tRNA^{Phe}_{Etd}$ in Solution. Analysis of the rotational motion provides additional information on the solution structure of $tRNA^{Phe}$. When an average rotational diffusion constant for all three states of $tRNA^{Phe}_{Etd}$ was estimated, a clear tendency appeared. The average rotational diffusion constant decreases when the $MgCl_2$ concentration increases (Table III). Dynamic light-scattering experiments indicate a large conformational change of $tRNA^{bulk}_{yeast}$ and $tRNA^{Phe}_{yeast}$ (Olson et al., 1976). The translational diffusion coefficient decreases 10% when the Mg^{2+} concentration increases from 1 to 10 mM, which is in qualitative agreement with our results (Table III).

Relating one rotational relaxation time to each lifetime always gives a higher tumbling rate for T_2 than for T_1 (Table IV). Unfortunately, the accuracy in the rotational relaxation time for T_3 is low because of a short fluorescence lifetime (Table IV) of this state and because of the small amplitude of the rotational part of the fluorescence decay. Interpreting the results of Table III by a shift in the distribution of states from T_1 and T_2 to T_3 requires that the state T_3 has a smaller tumbling rate than T_1 and T_2. One significant result pointing in this direction regards $tRNA^{Phe}_{Etd37B}$ (Table IV) where a long rotational relaxation time was found for T_3.

The analysis of the fluorescence lifetimes suggests ethidium to be stacked and fixed in T_1 and unstacked in T_3. Therefore, more local mobility is expected for T_3. This is confirmed by a small R value for this conformation, indicating that there is some reorientation of the ethidium which is faster than the time resolution of our instrument.

The tumbling rate of T_2 is higher that those of T_1 and T_3, indicating that T_2 represents the most compact conformation.

Rotational tumbling of $tRNA^{Phe}_{yeast}$ has been investigated previously with reversibly adsorbed ethidium bromide (Tao et al., 1970). Within the limited concentration range of Mg^{2+} used by these authors, our results agree with their data.

Structure of $tRNA^{Phe}$ in Solution and in the Crystal Lattice. It is reasonable to assume that one of the structural states T_1, T_2, or T_3 represents the tRNA structure found in the crystalline state. Besides $MgCl_2$, spermine was also a necessary component to crystallize tRNA both in the orthorhombic (Kim et al., 1971) and monoclinic form (Ladner et al., 1972). We found that by increasing the $MgCl_2$ concentration the probability of state T_3 increases to about 60% (Figures 2 and 3). Investigation of the binding of spermine to $tRNA^{Phe}_{Etd37}$ and $tRNA^{Phe}_{Etd16/17}$ reveals that spermine changes the distribution of T_1, T_2, and T_3 as does Mg^{2+} and together with Mg^{2+} is able to shift the probability of T_3 above 60% (L. Nilsson and R. Rigler, unpublished experiments). If we assume that the structural state with the highest probability is most likely to crystallize, this result indicates that the state T_3 might be closely related to or identical with the crystal structure.

Since state T_3 dominates in solution under conditions used for crystallization (Kim et al., 1971; Ladner et al., 1972), it is not surprising that little or no differences were found in the fluorescence of wybutine (Kim et al., 1975) or in Raman spectra (Chen et al., 1975) when $tRNA^{Phe}$ in the crystal and in the mother liquid are compared.

tRNA Structure and Function. The existence of different conformational states of tRNA has been postulated on the basis of results from phosphorylation experiments with polynucleotide kinase (Hänggi et al., 1970; Zachau et al., 1972) and from degradation experiments with polynucleotide phosphorylase (Thang et al., 1971). The data indicate that these different conformations go along with changes in the susceptibility of the acceptor end for enzymatic attack.

The existence of a Mg^{2+}- and spermine-dependent conformational change of $tRNA^{Ile}$ as a requirement for the acceptance of isoleucine has been deduced from enzyme kinetic studies (Lövgren et al., 1978). Our finding that Mg^{2+} and spermine are able to stabilize two conformations, an exfolded (T_3) and a more compact one (T_2), can have a direct connection with this observation. Fasiolo & Fersht (1978) report the transfer of phenylalanine from phenylalanine-AMP to $tRNA^{Phe}$ to be the rate-limiting step in the aminoacylation reaction. It occurs on the same time scale as the slow transitions between our states T_2 and T_3 and suggests that this conformational change might be an important step in the charging reaction. A compact tRNA conformation with aminoacyl and anticodon sites in close contact has been related to the recognition of tRNA by aminoacyl-tRNA synthetases (Reid, 1977) as well as to an unique assignment of the amino acid to the anticodon by primitive synthetases (Eigen & Schuster, 1978).

A change of the tRNA conformation upon binding to the ribosome has been suggested by the finding that the TΨCG sequence, which is engaged in intramolecular interactions in the crystal structure, seems to interact with the ribosome (Ofengand & Henes, 1969; Richter et al., 1974). It has been proposed that the exposure of the TΨCG sequence is triggered by the codon–anticodon interaction (Schwarz et al., 1976). Ribosome binding experiments using the fluorescent $tRNA^{Phe}$ derivatives also indicate a conformational change of the tRNA molecule when the complex with programmed ribosomes is formed (Robertson et al., 1977).

A static picture of tRNA in which the molecule forms a rigid and nonchanging unit must evidently be substituted by a dynamic concept. The biological functioning of tRNA requires several conformations, one of which is probably the X-ray structure present in the crystal. A detailed knowledge of these structural states and their transitions is needed for the understanding of specificity in the aminoacylation reaction, for the selection of aminoacyl-tRNAs by the elongation factor Tu and by the programmed ribosome.

Acknowledgments

We thank H. G. Zachau and L. Nilsson for stimulating discussions, R. Jakabffy and B. Larsson for expert technical assistance, and K. Dahlberg for typing the manuscript.

Appendix

Kinetic Description of Three Macromolecular States in Dynamic Equilibrium with Application to Fluorescence Measurements. A macromolecule can exist in the three states T_1, T_2, and T_3 which are in dynamic equilibrium. A ligand of free concentration c induces changes in the equilibrium distribution of the states and in the transition rates. It is assumed that the ligand binding is a fast process in relation to the conformational transitions. Then, quite generally, we can write for the slow time range of interest

$$T_2 \underset{k_{12}(c)}{\overset{k_{21}(c)}{\rightleftharpoons}} T_1 \underset{k_{31}(c)}{\overset{k_{13}(c)}{\rightleftharpoons}} T_3 \qquad \text{(A1)}$$

The influence of a pathway between T_2 and T_3 instead of between T_1 and T_3 is treated below. The ligand-dependent equilibrium constants are defined as

$$R(c) = \frac{[T_2]}{[T_1]} = \frac{k_{12}(c)}{k_{21}(c)}$$

$$L(c) = \frac{[T_3]}{[T_1]} = \frac{k_{13}(c)}{k_{31}(c)} \qquad \text{(A2)}$$

The relative concentrations

$$x_i = \frac{[T_i]}{\sum_{j=1}^{3}[T_j]}; \qquad i = 1, 2, \text{ and } 3 \qquad \text{(A3)}$$

are equivalent to the probabilities of the three states. Perturbations δx_i from the equilibrium probabilities x_i (i = 1, 2, and 3) will decay obeying the differential equations

$$\frac{\partial}{\partial t}\delta x_2(t) = -[k_{21}(c) + k_{12}(c)]\delta x_2(t) - k_{12}(c)\delta x_3(t)$$

$$\frac{\partial}{\partial t}\delta x_3(t) = -k_{13}(c)\delta x_2(t) - [k_{31}(c) + k_{13}(c)]\delta x_3(t) \qquad \text{(A4)}$$

where

$$\delta x_1(t) + \delta x_2(t) + \delta x_3(t) = 0 \qquad \text{(A5)}$$

A general solution to eq A4 may be obtained by a matrix algebra approach (Eigen & DeMaeyer, 1963). We assume, however, that the transition between, e.g., T_1 and T_2 is considerably faster than the transition between T_1 and T_3, a behavior which is observed for tRNA$^{Phe}_{Etd}$.

The variables $\delta x_1(t)$ and $\delta x_2(t)$ exhibit rapid relaxations according to

$$\delta x_2(t) = \delta x_2(0)e^{-t/\tau_{CH(2)}} - (1 - e^{-t/\tau_{CH(2)}})\frac{R(c)}{1 + R(c)}\delta x_3(0)$$

$$\delta x_1(t) = \delta x_1(0)e^{-t/\tau_{CH(2)}} - (1 - e^{-t/\tau_{CH(2)}})\frac{1}{1 + R(c)}\delta x_3(0) \qquad \text{(A6)}$$

where according to eq A5

$$\delta x_1(0) + \delta x_2(0) + \delta x_3(0) = 0$$

The chemical relaxation time $\tau_{CH(2)}$ is given by

$$1/\tau_{CH(2)} = k_{12}(c) + k_{21}(c) \qquad \text{(A7)}$$

Experimental knowledge of $\tau_{CH(2)}$ and $R(c)$ makes the determination of the two rate constants in eq A7 possible. From the definitions in eq A2 and A7

$$k_{12}(c) = (1/\tau_{CH(2)})\frac{R(c)}{1 + R(c)}$$

$$k_{21}(c) = (1/\tau_{CH(2)})\frac{1}{1 + R(c)} \qquad \text{(A8)}$$

At times considerably longer than $\tau_{CH(2)}$, the preequilibria

$$\delta x_2(t) = -\frac{R(c)}{1 + R(c)}\delta x_3(t)$$

$$\delta x_1(t) = -\frac{1}{1 + R(c)}\delta x_3(t) \qquad \text{(A9)}$$

are established. Introduction of eq A9 in the second equation in the system (eq A4) leads to the expression

$$\delta x_3(t) = \delta x_3(0)e^{-t/\tau_{CH(1)}} \qquad \text{(A10)}$$

where

$$1/\tau_{CH(1)} = \frac{k_{13}(c)}{1 + R(c)} + k_{31}(c) = k_{31}(c)\frac{1 + R(c) + L(c)}{1 + R(c)} \qquad \text{(A11)}$$

Experimental knowledge of $\tau_{CH(1)}$, $R(c)$, and $L(c)$ makes the determination of $k_{13}(c)$ and $k_{31}(c)$ possible:

$$k_{13}(c) = (1/\tau_{CH(1)})\frac{1 + R(c)}{1 + R(c) + L(c)}L(c)$$

$$k_{31}(c) = (1/\tau_{CH(1)})\frac{1 + R(c)}{1 + R(c) + L(c)} \qquad \text{(A12)}$$

The assumption in eq A1 that the slow transition occurs between states T_1 and T_3 is a priori arbitrary. Conceivable as well is a slow transition between T_2 and T_3 with the corresponding rate constants $k_{23}(c)$ and $k_{32}(c)$:

$$T_1 \underset{k_{21}(c)}{\overset{k_{12}(c)}{\rightleftharpoons}} T_2 \underset{k_{32}(c)}{\overset{k_{23}(c)}{\rightleftharpoons}} T_3 \qquad \text{(A13)}$$

The rate constants k_{23} and k_{32} may be obtained from eq A12 by replacing R with $1/R$ and L with L/R. Thus

$$k_{23}(c) = (1/\tau_{CH(1)})\frac{1 + R(c)}{1 + R(c) + L(c)}\frac{L(c)}{R(c)}$$

$$k_{32}(c) = (1/\tau_{CH(1)})\frac{1 + R(c)}{1 + R(c) + L(c)} \qquad \text{(A14)}$$

If the macromolecule T contains a fluorescent group whose lifetime τ is conformation sensitive, then it is possible to detect the states T_1, T_2, and T_3 (Rigler & Ehrenberg, 1976). The amplitude A_i, evaluated from pulsed fluorescence measurements, corresponding to the lifetime τ_i is given by eq 4

$$A_i = \text{constant } [T_i]\epsilon_i q_i^e; \qquad i = 1, 2, \text{ and } 3$$

If the product $\epsilon_i q_i^e$ is the same for i = 1, 2, and 3, the equilibrium constants $R(c)$ and $L(c)$ can be determined:

$$R(c) = \frac{[T_2]}{[T_1]} = \frac{A_2}{A_1}$$

$$L(c) = \frac{[T_3]}{[T_1]} = \frac{A_3}{A_1} \qquad \text{(A15)}$$

Furthermore, the probabilities x_i are given by

$$x_i = A_i/\sum_{j=1}^{3}A_j; \qquad i = 1, 2, \text{ and } 3 \qquad \text{(A16)}$$

Experimental detection of two chemical relaxation times, one short and one long, leaves three possibilities open regarding how the transitions shall be ascribed with respect to the spectroscopically identified conformations T_1, T_2, and T_3 with lifetimes τ_1, τ_2, and τ_3.

The fast relaxation might be between T_1 and T_2, between T_2 and T_3, or finally between T_1 and T_3. A way of resolving this question, so that the equilibrium information in eq A15 can be used unequivocally to obtain the kinetic constants according to eq A8 and A12, is to perform pulsed fluorescence measurements at the initial (T_{in}) and final (T_{fi}) temperatures of a temperature-jump series. The spectra of the relative amplitudes in the temperature jump can then be simulated according to the three kinetically different possibilities and compared with the actually measured amplitudes. According

to eq 5 the total fluorescence intensity is

$$I(c) = \text{constant} \cdot \sum_{i=1}^{3} A_i(c)\tau_i = \text{constant} \cdot \sum_{i=1}^{3} x_i(c)\tau_i$$

Define

$$\frac{\delta I}{I} = \frac{I_{in} - I_{fi}}{I_{fi}} = \frac{\delta I_1(0)}{I} + \frac{\delta I_2(0)}{I} \qquad \text{(A17)}$$

where I_{in} and I_{fi} are the total intensities before and after the temperature jump, respectively.

From eq 5 and A6 we obtain

$$\frac{\delta I_2(0)}{I} = \left[\delta x_2(0) + \frac{R(c)}{1 + R(c)} \delta x_3(0) \right] \times (\alpha_{12} - 1)/(x_2\alpha_{12} + x_1 + x_3\alpha_{13}) \qquad \text{(A18)}$$

where

$$\alpha_{12} = \tau_2/\tau_1$$
$$\alpha_{13} = \tau_3/\tau_1 \qquad \text{(A19)}$$

and where

$$\delta x_2(0) = x_2(T_{in}) - x_2(T_{fi})$$
$$\delta x_3(0) = x_3(T_{in}) - x_3(T_{fi}) \qquad \text{(A20)}$$

Similarly from eq A9 and A10

$$\frac{\delta I_1(0)}{I} = \delta x_3(0) \times \left[\alpha_{13} - 1 + \frac{R(c)}{1 + R(c)}(1 - \alpha_{12}) \right] \Big/ (x_2\alpha_{12} + x_1 + x_3\alpha_{13}) \qquad \text{(A21)}$$

All parameters in eq A18 and in eq A21 are now obtainable from pulsed experiments.

Two parameters of interest which influence the properties of the macromolecule T are the degree of ligand binding and the temperature. We assume that there are two types of intrinsically equivalent and independent binding sites for the ligand to each of the conformations. There are m strong (type 1) sites with association constants K_1, K_2, and K_3 and there are n weak sites (type 2) with association constants Q_1, Q_2, and Q_3 for the macromolecular conformations T_1, T_2, and T_3, respectively.

A more detailed version of reaction A1 is

$$\begin{array}{ccccc} T_{1(00)} & \underset{k_{21}(0)}{\overset{k_{12}(0)}{\rightleftharpoons}} & T_{2(00)} & \underset{k_{32}(0)}{\overset{k_{23}(0)}{\rightleftharpoons}} & T_{3(00)} \\ \vdots & & \vdots & & \vdots \\ T_{1(ij)} & \rightleftharpoons & T_{2(ij)} & \rightleftharpoons & T_{3(ij)} \\ \vdots & & \vdots & & \vdots \\ T_{1(mn)} & \rightleftharpoons & T_{2(mn)} & \rightleftharpoons & T_{3(mn)} \end{array} \qquad \text{(A22)}$$

The notation of $T_{1(ij)}$ signifies structure T_1 with i ligands bound of type 1 and j ligands bound to type 2. The concentration of a structure is given by summing the appropriate vertical in eq 22:

$$[T_i] = \sum_{k=1}^{m} \sum_{l=1}^{n} [T_{i(kl)}]; \qquad i = 1, 2, \text{ and } 3 \qquad \text{(A23)}$$

Using the binomial theorem we obtain for the equilibrium constant $R(c)$ in the special case (eq A22)

$$R(c) = \frac{[T_2]}{[T_1]} = R(0)\frac{(1 + K_2c)^m(1 + Q_2c)^n}{(1 + K_1c)^m(1 + Q_1c)^n} \qquad \text{(A24)}$$

Similarly

$$L(c) = \frac{[T_3]}{[T_1]} = L(0)\frac{(1 + K_3c)^m(1 + Q_3c)^n}{(1 + K_1c)^m(1 + Q_1c)^n} \qquad \text{(A25)}$$

On the further assumption, which essentially is an extension of the concept of equivalent and independent binding sites also to the kinetics, that each added ligand molecule influences the rate constants of a certain transition with the same factor, we obtain the general expressions

$$k_{12}(c) = k_{12}(0)\frac{(1 + p_1K_1c)^m(1 + q_1Q_1c)^n}{(1 + K_1c)^m(1 + Q_1c)^n}$$
$$k_{21}(c) = k_{21}(0)\frac{(1 + p_1K_1c)^m(1 + q_1Q_1c)^n}{(1 + k_2c)^m(1 + Q_2c)^n} \qquad \text{(A26)}$$

The kinetic factors p_1 and q_1 in eq A26, which can be any positive number, do not influence the equilibrium between T_1 and T_2. They contain information about how the reaction pathway is influenced by the ligand binding and are therefore important parameters in phenomena related to catalysis.

The rate constants for the slow transition are

$$k_{13}(c) = k_{13}(0)\frac{(1 + p_3K_1c)^m(1 + q_3Q_1c)^n}{(1 + K_1c)^m(1 + Q_2c)^n}$$
$$k_{31}(c) = k_{31}(0)\frac{(1 + p_3K_1c)^m(1 + q_3Q_1c)^n}{(1 + K_3c)^m(1 + Q_3c)^n} \qquad \text{(A27)}$$

p_3 and q_3 are the kinetic factors for the transition between T_1 and T_3. These results are generalizations of previous derivations by Eigen & DeMaeyer (1963).

Assuming instead that the slow transition occurs between states T_2 and T_3, the expressions

$$k_{23}(c) = k_{23}(0)\frac{(1 + p_2K_2c)^m(1 + q_2Q_2c)^n}{(1 + K_2c)^m(1 + Q_2c)^n}$$
$$k_{32}(c) = k_{32}(0)\frac{(1 + p_2K_2c)^m(1 + q_2Q_2c)^n}{(1 + K_3c)^m(1 + Q_3c)^n} \qquad \text{(A28)}$$

are obtained. p_2 and q_2 are the kinetic factors for the transition between states T_2 and T_3.

Adopting a formalism from transition-state theory [e.g., Laidler (1969)], giving the temperature dependence of the rate constants a thermodynamic interpretation, we write

$$k_{12}(c) = we^{(-\Delta H^*_{12}/RT)+(\Delta S^*_{12}/R)}$$
$$k_{21}(c) = we^{(-\Delta H^*_{21}/RT)+(\Delta S^*_{21}/R)} \qquad \text{(A29)}$$

and for the transition rates between T_1 and T_3

$$k_{13}(c) = we^{(-\Delta H^*_{13}/RT)+(\Delta S^*_{13}/R)}$$
$$k_{31}(c) = we^{(-\Delta H^*_{31}/RT)+(\Delta S^*_{31}/R)} \qquad \text{(A30)}$$

The enthalpy differences in eq A29 and A30 are defined according to

$$\Delta H^*_{ij} = H^*_{ij} - H(T_i); \qquad i,j = (1,2), (2,1), (1,3), \text{ and } (3,1) \qquad \text{(A31)}$$

where $H^*_{ij} = H^*_{ji}$ is the enthalpy at the top of the barrier for the transition between T_i and T_j and $H(T_i)$ is the enthalpy of the state T_i. A corresponding definition can be made for the entropy differences ΔS^*_{ij}. w is a frequency factor.

It should be noted that the definitions in eq A29 and A30 depend on all the parameters in eq A26 and A27, respectively.

References

Belford, G. G., Belford, R. L., & Weber, G. (1972) *Proc. Natl. Acad. Sci. U.S.A. 69*, 1392–1393.

Cameron, V., & Uhlenbeck, O. C. (1973) *Biochem. Biophys. Res. Commun. 50*, 535–640.

Chen, M. C., Giege, R., Lord, R. C., & Rich, A. (1975) *Biochemistry 14*, 4385–4391.

Chuang, T. J., & Eisenthal, K. B. (1972) *J. Chem. Phys. 57*, 5094–5097.

Ehrenberg, M. (1975) Thesis, Royal Institute of Technology, Stockholm, Sweden.

Ehrenberg, M., & Rigler, R. (1972) *Chem. Phys. Lett. 14*, 539–544.

Eigen, M., & DeMaeyer, L. (1963) *Tech. Org. Chem. 8* (Part II), 895–1054.

Eigen, M., & Schuster, P. (1978) *Naturwissenschaften 65*, 341–369.

Eisinger, J., & Spahr, P. F. (1973) *J. Mol. Biol. 73*, 131–137.

Erdmann, V. A., Sprinzl, M., & Pongs, O. (1973) *Biochem. Biophys. Res. Commun. 54*, 942–948.

Fasiolo, F., & Fersht, A. R. (1978) *Eur. J. Biochem. 85*, 85–88.

Grinvald, A., & Steinberg, I. Z. (1974) *Anal. Biochem. 59*, 583–598.

Hänggi, U. J., Streeck, R. E., Voigt, H. P., & Zachau, H. G. (1970) *Biochim. Biophys. Acta 217*, 287–293.

Holbrook, S., Sussman, J., Warrant, R., Church, G., & Kim, S. H. (1977) *Nucleic Acids Res. 4*, 2811–2820.

Jack, A., Ladner, J., Rhodes, D., Brown, R., & Klug, A. (1977) *J. Mol. Biol. 111*, 315–328.

Johnston, P. D., & Redfield, A. G. (1977) *Nucleic Acids Res. 4*, 3599–3615.

Johnston, P. D., & Redfield, A. G. (1978) *Nucleic Acids Res. 5*, 3913–3927.

Kan, L. S., Ts'o, P. O. P., Sprinzl, M., van der Haar, F., & Cramer, F. (1977) *Biochemistry 16*, 3143–3154.

Kim, S. H., Quigley, G., Suddath, F. L., & Rich, A. (1971) *Proc. Natl. Acad. Sci. U.S.A. 58*, 841–845.

Kim, S. H., Suddath, F. L., Quigley, G. J., McPherson, A., Sussman, J. L., Wang, A. H. J., Seeman, N. C., & Rich, A. (1974) *Science 185*, 435–440.

Kim, S. H., Langlois, R., & Cantor, Ch. (1975) *Abstracts, EMBO Workshop on tRNA Structure and Function*, Nof Ginossar, Israel.

Ladner, J. E., Finch, J. T., Klug, A., & Clark, B. F. C. (1972) *J. Mol. Biol. 72*, 99–101.

Ladner, J. E., Jack, A., Robertus, J. D., Brown, R. S., Rhodes, D., Clark, B. F. C., & Klug, A. (1975) *Proc. Natl. Acad. Sci. U.S.A. 72*, 4866–4870.

Laidler, K. J. (1969) *Theories of Chemical Reaction Rates*, McGraw-Hill, New York.

Leroy, J. L., Guéron, M., Thomas, G., & Favre, A. (1977) *Eur. J. Biochem. 74*, 567–574.

Lövgren, T. N. E., Petersson, A., & Loftfield, B. (1978) *J. Biol. Chem. 253*, 6702–6710.

Marquardt, D. W. (1963) *J. Soc. Ind. Appl. Math 11*, 431–441.

Meeter, D. A. (1964) *Non-Linear Least-Squares* (*Gaushaus*), University of Wisconsin Computing Center.

Ofengand, J., & Henes, P. (1969) *J. Biol. Chem. 244*, 6241–6253.

Olmsted, J., & Kearns, D. R. (1977) *Biochemistry 16*, 3647–3654.

Olson, T., Fournier, M. J., Langley, K. H., & Ford, N. C. (1976) *J. Mol. Biol. 102*, 193–203.

Quigley, G. J., Teeter, M., & Rich, A. (1978) *Proc. Natl. Acad. Sci. U.S.A. 75*, 64–68.

Reid, B. R. (1977) in *Nucleic Acid–Protein Recognition* (Vogel, H. J., Ed.) pp 375–390, Academic Press, New York.

Richter, D., Erdmann, V. A., & Sprinzl, M. (1974) *Proc. Natl. Acad. Sci. U.S.A. 71*, 3226–3229.

Rigler, R., & Ehrenberg, M. (1973) *Q. Rev. Biophys. 6*, 139–199.

Rigler, R., & Ehrenberg, M. (1976) *Q. Rev. Biophys. 9*, 1–19.

Rigler, R., Rabl, C. R., & Jovin, T. M. (1974) *Rev. Sci. Instrum. 45*, 580–588.

Rigler, R., Ehrenberg, M., & Wintermeyer, W. (1977) in *Molecular Biology, Biochemistry and Biophysics* (Pecht, I., & Rigler, R., Eds.) Vol. 24, pp 219–244, Springer-Verlag, Heidelberg.

Robertson, J. M., Kahan, M., Wintermeyer, W., & Zachau, H. G. (1977) *Eur. J. Biochem. 72*, 117–125.

Römer, R., & Hach, R. (1975) *Eur. J. Biochem. 55*, 271–284.

Schwarz, U., Menzel, H. M., & Gassen, H. G. (1976) *Biochemistry 15*, 2484–2490.

Stein, A., & Crothers, D. M. (1976) *Biochemistry 15*, 157–159.

Tao, T., Nelson, J. H., & Cantor, Ch. R. (1970) *Biochemistry 9*, 3514–3524.

Thang, M. N., Beltchev, B., & Grunberg-Manago, M. (1971) *Eur. J. Biochem. 19*, 184–193.

Thiebe, R., & Zachau, H. G. (1969) *Methods Enzymol. 20*, 179–182.

Uhlenbeck, O. C. (1972) *J. Mol. Biol. 65*, 25–41.

Urbanke, C., & Maass, G. (1978) *Nucleic Acids Res. 5*, 1551–1560.

Walters, J., Geerdes, H., & Hilbers, C. (1977) *Biophys. Chem. 7*, 147–151.

Wintermeyer, W., & Zachau, H. G. (1971) *FEBS Lett. 18*, 214–218.

Wintermeyer, W., & Zachau, H. G. (1974) *Methods Enzymol. 29*, 667–673.

Wintermeyer, W., & Zachau, H. G. (1975a) *FEBS Lett. 58*, 306–309.

Wintermeyer, W., & Zachau, H. G. (1975b) *Mol. Biol.* (*Moscow*) *9*, 49–53.

Wintermeyer, W., & Zachau, H. G. (1979) *Eur. J. Biochem. 98*, 465–475.

Wintermeyer, W., Schleich, H. G., & Zachau, H. G. (1979a) *Methods Enzymol. 59*, 110–121.

Wintermeyer, W., Robertson, J. M., Weidner, H., & Zachau, H. G. (1979b) in *Transfer RNA. Structure, Properties, and Recognition* (Abelson, J., Schimmel, P., & Söll, D., Eds.) pp 445–457, Cold Spring Harbor, New York.

Zachau, H. G., Streeck, R. E., & Hänggi, U. J. (1972) in *Gene Expression and its Regulation* (Kenney, T., Hamkalo, B. A., Favelukes, G., & August, J. T., Eds.) pp 217–228, Plenum Press, New York.